EDGE ARTICLE

Check for updates

Insights into the role of noncovalent interactions in distal functionalization of the aryl C(sp^2)–H bond†

Anju Unnikrishnan [ID] and Raghavan B. Sunoj [ID] *

Burgeoning interest in distal functionalization of aryl C–H bonds led to the development of iridium-catalyzed borylation reactions. The significance and inadequate mechanistic understanding of C(sp^2)–H borylations motivated us to investigate the key catalytic steps and the origin of a directing-group-free regiocontrol in the reaction between aryl amides and B$_2$pin$_2$ (bis(pinacolato)diboron). An Ir(III)(ubpy) tris(boryl) complex, generated from the pre-catalyst [Ir(OMe)(cod)]$_2$ by the action of a bipyridine-urea ligand (ubpy) and B$_2$pin$_2$, is considered as the most likely active catalyst. The *meta* C–H activation of *N,N*-dihexylbenzamide is energetically more favorable over the *para* isomer. The origin of this preference is traced to the presence of a concerted action of noncovalent interactions (NCIs), primarily between the catalyst and the substrate, in the regiocontrolling transition states (TSs). Molecular insights into such TSs revealed that the N–H⋯O interaction between the tethered urea moiety of the Ir-bound ubpy ligand of the catalyst and the amide carbonyl of the substrate is a critical interaction that helps orient the *meta* C–H bond nearer to iridium. Other NCIs such as C–H⋯π between the substrate and the catalyst, C–H⋯O involving the substrate C–H and the oxygen of the B$_2$pin$_2$ ligand and C–H⋯N between the substrate and the N atom of the Ir-bound ubpy confirm the significance of such interactions in providing the desirable differential energies between the competing TSs that form the basis of the extent of regioselectivity.

Introduction

Selective activation of thermodynamically strong and kinetically inert C–H bonds has garnered the attention of chemists for decades. Among the several activation strategies available, functionalization *via* C–H bond activation using a borylation reaction is a promising one due to the wider utility of the borylated products.[1] The C–H borylation reactions witnessed a number of interesting developments encompassing a range of transition metals such as Co, Ni, Ru, Rh, Pd and Ir.[2] Some of the most important examples in this genre employ iridium catalysts in conjunction with the prototypical B$_2$pin$_2$ (bis(pinacolato)diboron) as the borylating agent. In this regard, use of pre-catalysts such as [Ir(X)(cod)]$_2$ (where X = Cl and OMe) and bipyridine ligands in the activation of the C(sp^2)–H bond is noteworthy.[3]

A lot of effort has been expended toward developing selective activation of aryl C–H bonds, wherein one typically strives to achieve control over *ortho*, *meta* and *para* functionalization. The functional group (FG) directed borylation is an effective protocol for imparting *ortho* selectivity.[4] Along the similar lines, efforts for achieving *meta* selectivity[5] continued to receive

attention due to the synthetic value of the *meta* functionalized products.[6] Development of a functionalization strategy without having to use an additional directing group (DG) on the substrate, is certainly a great advantage.[7] It will, therefore, be of inherent value if the catalyst could perform the directing role such that the method can be utilized for a broader range of substrates.[8] Such an approach would help reduce the proportion of a DG from stoichiometric to catalytic levels. A number of such endeavors where the catalyst is tailored to perform the role of a directing group rely on the careful control/use of weak noncovalent interactions (NCIs).[9] Harnessing NCIs as a handle to gain regiocontrol in transition metal catalyzed C–H activation reactions remains much less explored at this stage of development. NCIs when operating in a concerted manner are known to impact the stereochemical outcome of reactions,[10] which is an idea that could be exploited in the catalyst design for regioselective transformations as well. Within the NCI directed C–H functionalization strategies, two distinct methods employing [Ir(OMe)(cod)]$_2$ and bipyridine-derived ligands as the catalytic system have been reported very recently. While the approach developed concurrently by Kanai[11] and Chattopadhyay[12] proposes a secondary interaction as responsible for directed C–H functionalization, the other one by Phipps demonstrated an ion-pair directed regiocontrol.[13]

In keeping with our continued efforts in probing the mechanism and selectivity controlling factors in transition metal

Department of Chemistry, Indian Institute of Technology Bombay, Powai, Mumbai 400076, India. E-mail: sunoj@chem.iitb.ac.in

† Electronic supplementary information (ESI) available: Optimized geometries and additional schemes, figures, and tables as described in the text along with the Cartesian coordinates are provided. See DOI: 10.1039/c8sc05335a
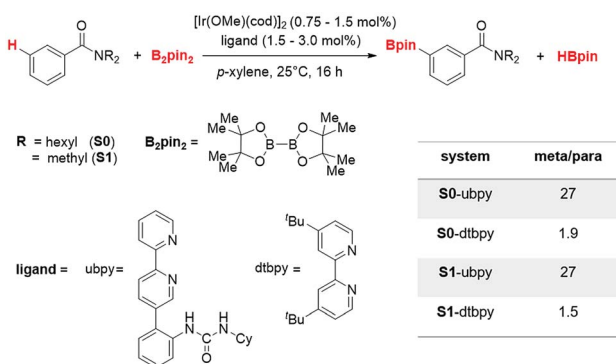
Scheme 1 Iridium(III)-catalyzed *meta* C(sp²)–H borylation of aryl amides using B_2pin_2.

catalyzed C–H functionalization reactions,[14] we became interested in examining the important *meta* C(sp²)–H borylation of aryl amides using [Ir(OMe)(cod)]₂ (Scheme 1). The observed regioselective borylation was proposed to arise from a hydrogen bonding interaction between the catalyst and the substrate.[15] Although the experimental studies on iridium catalyzed *ortho* borylation reactions are widely available, the current mechanistic understanding of *meta* C–H borylation is inadequate. Furthermore, rationalization of regioselectivity in these reactions typically invoked qualitative geometric features of certain putative intermediates or that of a transition state (TS) in a proposed mechanistic pathway. Hence, a number of vital geometric and energetic aspects responsible for the observed product distribution remain vague at this stage. Using DFT computations (SMD$_{(p\text{-xylene})}$/B3LYP-D3/6-31G**,SDD(Ir)), we aim to gain insights into (a) the energetic details of the catalytic cycle, (b) molecular geometry as well as electronic features of the critical intermediates and TSs, (c) the origin of regioselectivity, and (d) how changes in the substituents of the catalyst and/or substrate could impact the regiochemical outcome. The knowledge on the origin of regioselectivity would help make more rational modifications to the substrate and/or ligand as well as to expand the scope of such catalytic reactions.

Computational methods

All computations were performed using the Gaussian09 (Revision D.01) suite of quantum chemical programs.[16] We employed the hybrid density functional B3LYP[17] with Grimme's dispersion correction (D3)[18] in combination with the Stuttgart-Dresden double-ζ zeta basis set (SDD)[19] with an effective core potential for 60 inner electrons out of 77 total electrons for iridium and the 6-31G** basis set[20] for all the other elements. Similar computational methods were successfully employed in the study of transition metal catalyzed reactions.[21] All stationary points identified as TSs were characterized by one and only one imaginary frequency that corresponds to the expected reaction coordinate. The intrinsic reaction coordinate (IRC) calculations[22] were also done at the same level of theory to examine whether the TS is connected to the reactant/product as desired. The effect of the solvent was taken into account using the SMD

solvation model in *para*-xylene as the continuum dielectric ($\varepsilon = 2.27$).[23] The free energies of all the TSs and intermediates reported in the manuscript were obtained by adding the thermal and entropic corrections with the quasi rigid-rotor harmonic oscillator approximation[24] to the electronic energies in the condensed phase. Thus, the results and discussion are presented using the Gibbs free energies obtained at the SMD$_{(p\text{-xylene})}$/B3LYP-D3/6-31G**,SDD(Ir) level of theory at 298.15 K and 1 atm pressure, unless stated otherwise. Topological analyses of the electron densities were performed using Bader's Atoms-in-Molecules (AIM) using the AIM2000 software so as to analyze the weak inter-atomic interactions in various TSs.[25] Further, the regions of attractive and repulsive interactions are identified through the generation of NCI plots.[26] The energy span of the catalytic cycle has been calculated using the energetic span model developed by Shaik and Kozuch.[27]

Results and discussion

The catalytic regioselective borylation of C(sp²)–H bonds of aromatic amides using B₂pin₂ (bis(pinacolato)diboron), employing [Ir(OMe)(cod)]₂ as the pre-catalyst (cod = 1,5-cyclo-octadiene) in the presence of a bipyridine-derived ligand, is examined (Scheme 1). The ligand employed here is a urea-bpy (ubpy) system tethered *via* an *ortho*-phenylene linker. The Ir(III)(ubpy)tris(boryl) complex formed by the action of the ubpy ligand and the borylating agent B₂pin₂ on the pre-catalytic Ir(I) species is considered as the active catalyst.[3b,28] While different possible configurations of the active catalyst as well as that of the catalyst–substrate complex are first examined using a model system, all species involved in the catalytic cycle presented in the manuscript employ only the real system.[29]

1. Important details of the catalytic cycle

The key mechanistic steps in the overall catalytic cycle, starting with the formation of a catalyst–substrate complex are shown in Scheme 2. To generate adequate space to accommodate the substrate near the iridium center, a higher energy configuration (**A2**) of the active catalyst is considered.[30] Depending on the site of interaction of the substrate with the catalyst, three distinct coordination modes, such as an Ir···π (when the aromatic amide is coordinated through the aryl π ring), Ir···N (nitrogen of the amide) and Ir···O (carbonyl oxygen of the amide) binding, are examined.[31]

The computed energies suggest that the substrate coordination to the iridium center *via* oxygen or nitrogen atom of the amide group is equally feasible as they differ only by a kcal mol⁻¹.[32] The optimized geometries of the catalyst–substrate complexes in both these binding modes convey that only the *ortho* aryl C–H bond is close enough to the iridium center for any effective interaction. In other words, when *N,N*-dihexylbenzamide is bound to the catalyst through its amide moiety, the *meta* and *para* positions remain far from the iridium center to afford C–H bond activation.[33] In the π-binding mode, on the other hand, all the three aryl C–H bonds, including the *meta* enjoy enhanced proximity to the iridium center that can lead to
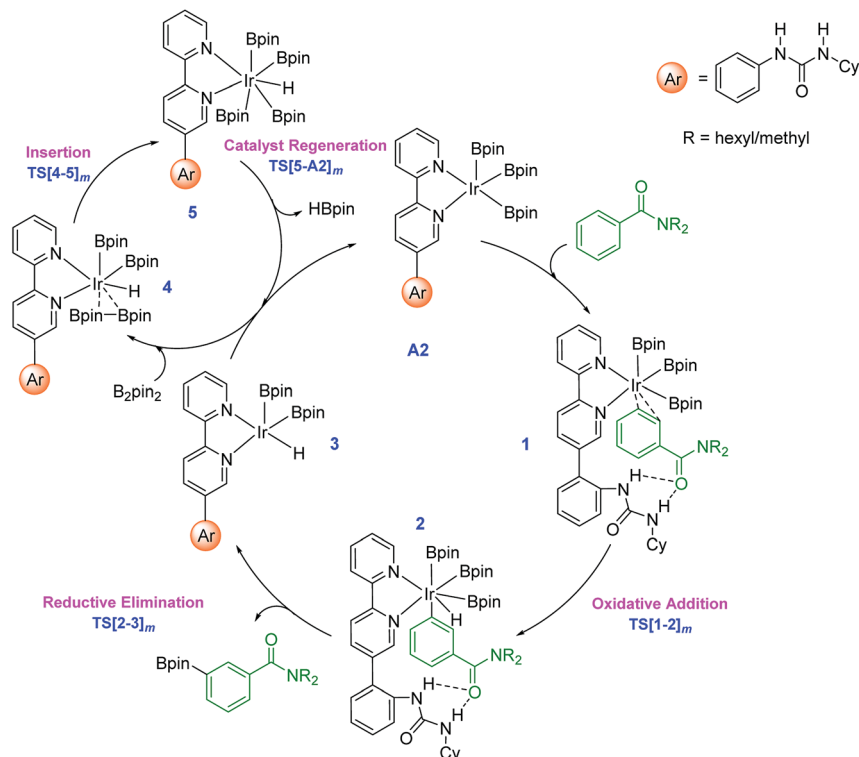
Scheme 2 Important mechanistic steps in the catalytic cycle for the Ir(III)-catalyzed borylation of aryl amides through C−H activation. The subscript m in the TS notation indicates the *meta* isomer.

effective functionalization.[34] Thus, the π-binding mode in the catalyst–substrate complex is considered as the reactive conformer in our study as shown in Scheme 2.

Since the *N*-hexyl chains are conformationally flexible, as many as 8 conformers of all the important TSs are identified.[35] The results presented herein are on the basis of the most favorable geometry for both the *meta* and *para* C–H activation TSs. The key mechanistic events in the catalytic cycle, as shown in Scheme 2, start with an oxidative addition in the catalyst–substrate complex **1** wherein Ir(III) inserts into the *meta* C–H bond *via* transition state **TS[1-2]**$_m$. The ensuing Ir(v)-aryl intermediate **2** then undergoes a reductive elimination (RE) through **TS[2-3]**$_m$ to generate the borylated product and an Ir(III)-hydride intermediate (**3**). Uptake of one molecule of B_2pin_2 by **3** can then lead to a weakly interacting complex between **3** and B_2pin_2, which is denoted as **4**. In the following step, insertion of B_2pin_2 into **4** generates a hepta-coordinate Ir(v) species (**5**) *via* **TS[4-5]**$_m$. The catalyst regeneration can be completed by the expulsion of a molecule of HBpin through the RE transition state **TS[5-A2]**$_m$. The active catalyst **A2**, thus generated, can then sustain the catalytic cycle by the uptake of another molecule of the substrate.[36]

The Gibbs free energy profile for the formation of the *meta* borylated product is provided in Fig. 1. The formation of the borylated product exhibits notable barriers of 21.6 and 21.5 kcal mol^{-1}, respectively, for the C–H activation and the RE. According to the energetic span model,[27] intermediate **1** and **TS[1-2]**$_m$ are, respectively, the turnover determining intermediate

(TDI) and turnover determining transition state (TDTS). The activation span (δE), calculated as the energy difference between the TDTS and TDI, is found to be 21.6 kcal mol^{-1}.[37] The subsequent steps in the mechanism, such as the B_2pin_2 insertion and the catalyst regeneration, are much less energy demanding, as indicated by their relatively lower barriers.

2. Factors controlling regioselectivity

The knowledge of energetics, geometry, and electronic features of the important TSs involved in a catalytic cycle would be valuable toward developing a better understanding of the catalytic transformation. For the present example, such features of the regio-controlling TSs enabling *meta* C–H activation are not established yet. Kanai's insightful working hypothesis,[15] on the other hand, placed a significant emphasis on the H-bonding between *N,N*-dialkylbenzamide and the urea moiety of the Ir-bound ubpy ligand as the key factor in their proposed TSs. The observed *meta* to *para* ratio of 27 corresponds to a selectivity of 93% in favor of *meta* borylation. To probe this important observation in greater depth, TSs for the *meta* and *para* C–H activation of substrates such as *N,N*-dihexylbenzamide (**S0**) and *N,N*-dimethylbenzamide (**S1**) are identified. Different variations in the catalyst (ubpy), and the borylating agent (**B0**) are also considered in this study. The original catalyst–substrate combination is referred to as ubpy-**S0** while that with a modified substrate is denoted as ubpy-**S1**. Optimized geometries of the regiocontrolling TSs for **S0** and **S1** are provided in Fig. S2 in the ESI.† Interestingly, two crucial N–H···O H-bonding interactions
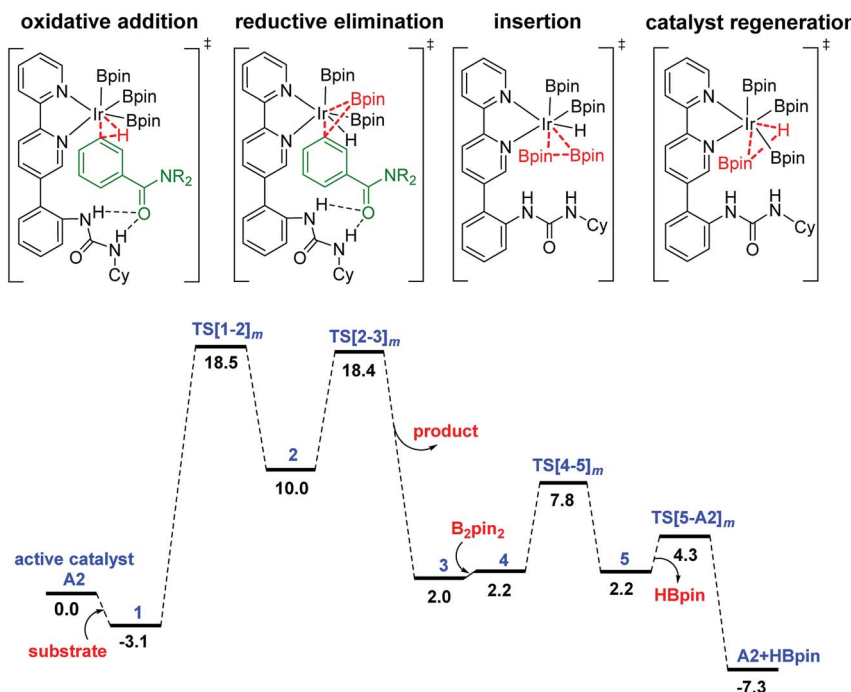
Fig. 1 Free energy profile of the Ir(III)-catalyzed *meta* C–H activation reaction. The subscript *m* in the TS notation indicates the *meta* isomer.

between the N–H of the urea and the oxygen atom of the amide (shown as v and w in Fig. 2) are noticed in the *meta* C–H activation transition states $TS[1-2]_{m(S0)}$ and $TS[1-2]_{m(S1)}$. However, only one such interaction (v) is found in the case of *para* C–H activation TSs ($TS[1-2]_{p(S0)}$ and $TS[1-2]_{p(S1)}$) with both the substrates. More important clues on regioselectivity could be gathered from these TSs through a comparison of other non-covalent interactions such as C–H⋯π, C–H⋯O and C–H⋯N besides the N–H⋯O H-bonding. An approximate estimate of the strength of these weak NCIs is calculated by using the values of the electron densities at the respective bond critical points (ρ_{bcp}) as obtained through Bader's AIM analysis.[25]

A summary of topological analysis of the electron density for $TS[1-2]_m$ and $TS[1-2]_p$ in the case of both ubpy-**S0** and ubpy-**S1** catalyst–substrate combinations, together with important interatomic distances, is given in Fig. 2. It can be noticed that in $TS[1-2]_{m(S0)}$ both the *N*-hexyl arms of the substrate are involved in multiple C–H⋯π interactions (shown as a, b, c, d, and e) with the catalyst through the aryl π-face of the Ir-bound ligands (*i.e.*, bpy ligand as well as with the phenyl-urea linker). Additionally, the cyclohexyl ring (Cy) attached to the urea moiety also participates in C–H⋯π interaction (f) with the substrate in **TS** $[1-2]_{m(S0)}$. On the other hand, in the *para* C–H activation transition state $TS[1-2]_{p(S0)}$, the relative orientation of the substrate is such that the C–H⋯π interaction with the catalyst is absent. Another significant NCI in $TS[1-2]_{m(S0)}$ is the C–H⋯O interaction between the aryl C–H of the substrate and B₂pin₂ (shown as h). Other C–H⋯O contacts denoted as g, i, j, k and l in $TS[1-2]_{m(S0)}$ represent the interactions between the ligands (Ir-bound bpy, phenyl-urea linker and Bpin). An equally good number of C–H⋯O interactions (g, i, m, n, o and p) are also noticed in the $TS[1-2]_{p(S0)}$. However, the overall number of NCIs is found to be

higher and they are relatively more efficient in $TS[1-2]_{m(S0)}$ than those in $TS[1-2]_{p(S0)}$ for the ubpy-**S0** combination.

Although the above-mentioned analysis, based on the difference in the number of NCIs, offers a qualitative insight into the origin of *meta* selectivity, it does not provide room for quantitative assessment. For instance, a lesser number of more efficient interactions can outweigh the influence of a greater number of weaker interactions. Hence, we endeavored to quantify the important NCIs using the topological parameters such as the electron density at the bond critical point (ρ_{bcp}), the corresponding Laplacian of the electron density ($\nabla^2\rho$), and kinetic energy (G) using Espinosa's formulation.[38] Although Espinosa's formulation was proposed for the quantification of isolated pairwise intermolecular H⋯F interactions, we have extended the same to various intramolecular weak NCIs operating in important TSs in the present study. Even though the formulation has not been applied to complex intramolecular interactions such as that prevail in regiocontrolling TSs, we believe that it could provide a reasonable measure of the relative strengths of the NCIs such as C–H⋯π, C–H⋯O, C–H⋯N and N–H⋯O. While a detailed mapping of the NCIs in $TS[1-2]_m$ and $TS[1-2]_p$ for both the ubpy-**S0** and ubpy-**S1** pairs is given in the ESI,†[39] herein a succinct representation of the major NCIs such as C–H⋯π, C–H⋯O, C–H⋯N and N–H⋯O is provided. It can be gleaned from the bar diagram, as given in Fig. 3, that each type of NCI has a different contribution in different catalyst–substrate systems.

Since the dihexyl chain of the substrate engages in a good number of C–H⋯π interactions with the catalyst, we wanted to examine whether changes in such interactions might affect the extent of regioselectivity. To this end, a modified substrate **S1** is considered wherein the *N,N*-dihexyl group on the amido
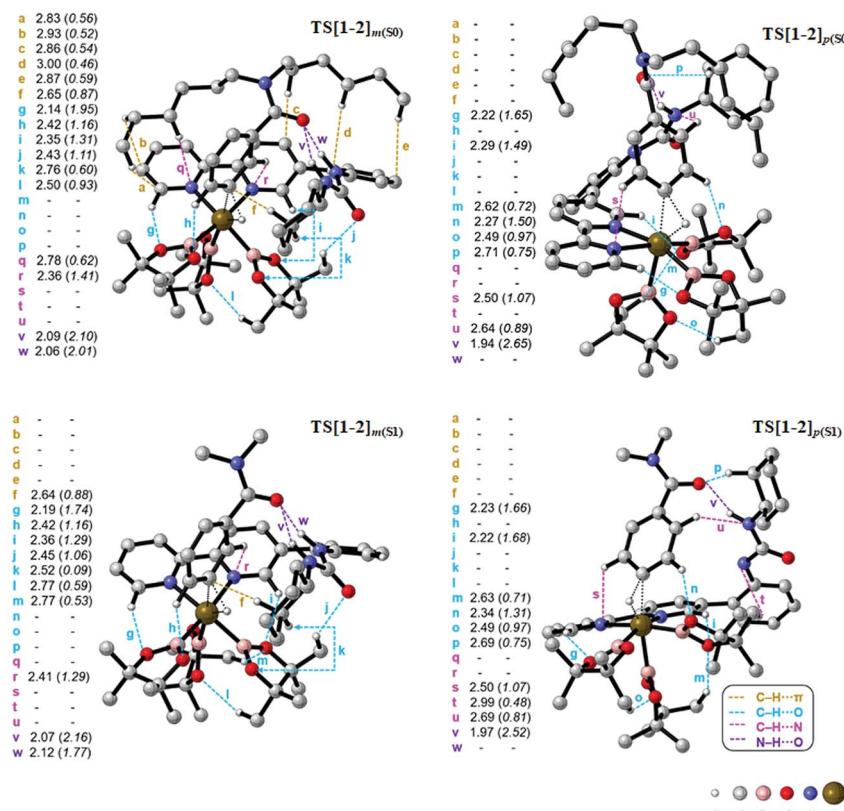
Fig. 2 Optimized geometries of the TSs for the *meta* and *para* C–H activation of ubpy-**S0** and ubpy-**S1** catalyst–substrate combinations. The distances are in Å and electron densities ($\rho \times 10^{-2}$ au) at the bond critical points are given in parentheses. The hydrogen atoms that are not involved in any noticeable interaction are removed for improved clarity.

nitrogen is replaced with a *N,N*-dimethyl substituent. The optimized transition state geometries are devoid of C–H⋯π interactions, except one such prominent contact between the cyclohexane of the urea moiety and the aryl group of the substrate (shown as f in Fig. 2). This interaction is present only in the case of **TS[1-2]**$_{m(S1)}$ but not in **TS[1-2]**$_{p(S1)}$. Interestingly, a number of other NCIs such as C–H⋯O and C–H⋯N interactions are found to be present in both the *meta* and *para* TSs for *N,N*-dimethyl amide as the substrate. It is also of interest to note

that the NCIs in the case of the **S1** system are not as pronounced as those in **S0** (Fig. 3). Further, the total strength of all the important NCIs is estimated to be −70.9 kcal mol^{-1} for **TS[1-2]**$_{m(S1)}$ and only −63.5 kcal mol^{-1} for **TS[1-2]**$_{p(S1)}$. The regioselectivity, calculated using the energy difference of 7.4 kcal mol^{-1} between the competing *meta* and *para* C–H activation TSs for the *N,N*-dimethylamide is strongly in favor of the *meta* isomer.

The summary of noncovalent interactions shown in Fig. 3 conveys that except for the C–H⋯O contacts, all the other NCIs
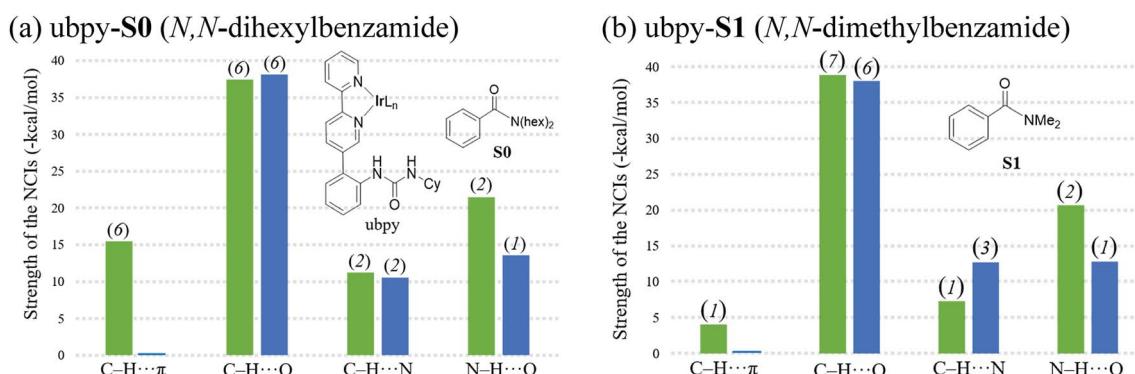

Fig. 3 Comparison of the sum of interaction energies of the NCIs in the *meta* (green) and *para* (blue) C–H activation TSs for (a) substrates **S0** and (b) **S1**. Values in parentheses above the bar diagrams are the number of noncovalent interactions.

are more dominant in **TS[1-2]**$_{m(S0)}$ (shown in green) than in **TS[1-2]**$_{p(S0)}$ (blue) for the ubpy-**S0** catalyst–substrate pair. It should be noted that **TS[1-2]**$_{m(S0)}$ is 6.6 kcal mol^{-1} lower in energy than **TS[1-2]**$_{p(S0)}$, suggesting that the NCIs do have a direct influence on the extent of regioselectivity. In the case of the **S1** system, though the number of C–H⋯π contacts is much smaller, other NCIs such as C–H⋯O and N–H⋯O interactions are able to effectively make **TS[1-2]**$_{m(S1)}$ lower in energy by 7.4 kcal mol^{-1} as compared to **TS[1-2]**$_{p(S1)}$. Thus, it appears that the C–H⋯π interactions may not solely be responsible for the observed high regioselectivity if the cumulative effect of other weak interactions is able to compensate.

It is also interesting to note that the difference in the total strength of NCIs between *meta* and *para* C–H activation TSs exhibits a good correlation with the predicted regioselectivity. The predicted preference toward the *meta* C–H activation for ubpy-**S0** and ubpy-**S1** is, respectively, 6.6 and 7.4 kcal. This is in line with the experimentally observed *meta* to *para* ratio of 27 for both the catalyst–substrate pairs. Appreciable difference in the collective strength of NCIs between the *meta* and *para* C–H activation TSs is noted in the case of ubpy-**S0** (23.4 kcal mol^{-1}) and ubpy-**S1** (7.4 kcal mol^{-1}), thus favoring *meta* C–H activation over the alternative *para* pathway. Hence, a combination of C–H⋯π, C–H⋯N and C–H⋯O interactions together with the N–H⋯O H-bonding makes the *meta* C–H activation TS lower in energy than the corresponding *para* position.[40]

While it is prudent to acknowledge that various noncovalent interactions described above impact the predicted relative energy order between the regiocontrolling TSs, analysis of the effect of distortion in such TSs is equally important. The Distortion–Interaction/Activation-Strain (DI-AS) analysis[41] was therefore carried out on these TSs to gain additional insights into the factors responsible for the observed regioselectivity. It can be noticed from the data provided in Table 1 that in both ubpy-**S0** and ubpy-**S1** catalyst–substrate combinations, the *para* C–H activation TSs experience a higher total distortion relative to the corresponding *meta* analogue. The extent of distortion in the substrate, as well as the catalyst in the *para* TS, is found to be higher than that in the *meta* case for ubpy-**S1**.[42] Thus, due to the combined effect of the higher number of NCIs operating in concert as well as the relatively lower distortion experienced by both the *meta* TSs, we could rationalize the preference toward the high *meta* regioselectivity in both the above-mentioned examples.

3. Rational modifications to change the pattern of NCIs

After having understood the critical role of various NCIs as well as the N–H⋯O H-bonding in the C–H activation step, we considered two new modifications of the parent system. As the N–H⋯O interactions were also found to play a vital role in imparting selectivity, the parent ligand ubpy is modified by removing the phenylene-urea linker to a simple bpy. Similarly, instead of B$_2$pin$_2$ (**B0**), we have considered B$_2$(OMe)$_4$ (**B1**) as the borylating agent.[43] The change in the regioselectivity due to these modifications is predicted for the substrate **S0**. The bpy ligand led to no energy difference between the *meta* and *para* C–H activation TSs, implying no regioselectivity. In other words, turning off the vital N–H⋯O interactions between the substrate and the catalyst, by way of removing the urea moiety diminishes the energetic advantage toward the *meta* C–H activation as compared to the competing *para* analogue.[44] Similar to the case with the bpy ligand, the **B1** modification also leads to a relatively smaller energy difference between the *meta* and *para* TSs (2.6 kcal mol^{-1}) compared to the unmodified system (6.6 kcal mol^{-1}).[45] A similar trend in selectivity is also noticed when computed using relative enthalpy differences between the *meta* and *para* TSs for the aforesaid modifications.[46] A detailed analysis of the *meta* and *para* C–H activation TSs of these modified systems based on Espinosa's formulation[47] and the DI-AS analysis[48] is thus performed to assess how NCIs impact the regiochemical outcome of this reaction.

We note that the prominent NCIs other than the N–H⋯O H-bonding in these modified systems are the C–H⋯O and C–H⋯N interactions. A quantified NCI, as given in Table 2, conveys that for the bpy modification, the total strength of the C–H⋯O interactions in **TS[1-2]**$_{p(bpy)}$ (−36.7 kcal mol^{-1}) is higher than that in the *meta* TS (−31.3 kcal mol^{-1}), while **TS[1-2]**$_{m(bpy)}$ enjoys improved C–H⋯N interaction (−8.9 kcal mol^{-1}) than in the *para* counterpart (−5.5 kcal mol^{-1}) (Table 2).[47] While the predicted strength of the C–H⋯O interactions appears to be overestimated, it serves the present purpose wherein we intend to compare the relative strengths of such interactions in chemically identical *meta* and *para* C–H activation TSs. Another interaction, namely, the N–H⋯O interaction is absent in both the TS geometries, and four more C–H⋯π interactions (−9.8 kcal mol^{-1}) are found in the *meta* TS than that in the *para* TS.

Table 1 Distortion energies (in kcal mol^{-1}) obtained through the distortion–interaction/activation-strain (DI-AS) analysis for the *meta* and *para* C–H activation transition states for ubpy-**S0** and ubpy-**S1**

System	ΔE_{dis} (ζ)		
	Substrate	Catalyst	Total in the TS
ubpy-**S0** (*meta*)	58.9	23.4	107.8
ubpy-**S0** (*para*)	58.8	25.4	109.2
ubpy-**S1** (*meta*)	56.0	22.8	100.0
ubpy-**S1** (*para*)	62.5	25.5	107.3

Table 2 Comparison of the strength^a of important noncovalent interactions (in kcal mol^{-1}) quantified using the electron density topological features in the C−H activation transition states with **S0** as the substrate

System	C–H⋯π	C–H⋯O	C–H⋯N	N–H⋯O
meta				
bpy-**B0**	−9.8	−31.3	−8.9	—^{b}
ubpy-**B1**	−13.6	−37.8	−11.9	−24.8
para				
bpy-**B0**	—^{b}	−36.7	−5.5	—^{b}
ubpy-**B1**	−4.8	−48.1	−9.3	−16.7

^{a} Sum of the strength of key NCIs (in kcal mol^{-1}) calculated using Espinosa's method. ^{b} This interaction is absent.

Thus, the absence of some of the important NCIs in **TS[1-2]**$_{m(bpy)}$ and **TS[1-2]**$_{p(bpy)}$ appears to result in comparable energies for both these TSs, which in turn, leads to very low regioselectivity.[47] In the case of **B1** modification, equal numbers of C–H···O interactions are identified in both *meta* and *para* TSs, albeit the cumulative strength of such interactions is higher in *para* (-48.1 kcal mol^{-1}) than that in *meta* (-37.8 kcal mol^{-1}) TS. However, a greater number of stronger N–H···O interactions are found in the *meta* TS than in *para* (Table 2). The C–H···N interactions, on the other hand, are found to be of comparable strengths in the *meta* (-11.9 kcal mol^{-1}) and *para* C–H activation TSs (-9.3 kcal mol^{-1}). The lack of notable differences in the noncovalent interactions can be regarded as the origin of the small energy difference (2.6 kcal mol^{-1}) between the two competing TSs.[47]

The *ortho* conundrum. The experiments suggested the formation of *meta* and *para* borylated products, but no *ortho* product.[15] This is somewhat surprising as no particular rationale was offered as to why an *ortho* borylated product was not observed. In principle, all the three C–H bonds at *ortho*, *meta* and *para* positions could be accessible for the oxidative addition. In line with this expectation, our computed data indicate that the C–H activation at the *ortho* position is more favorable than that at the *para* position. Importantly, the *meta* C–H activation is energetically the most favorable possibility, followed by *ortho* and then *para* activations. The barriers for the C–H activation step with respect to the respective preceding intermediates are found to be 21.6, 23.8 and 25.3 kcal mol^{-1}, respectively, for *meta*, *ortho*, and *para* positions. To inspect whether this predicted preference arises due to the use of a particular computational approach, we have also computed the Gibbs free energies using a range of different density functionals and basis sets.[49] All such additional computations yielded similar energetic trends, suggesting that the *ortho* C–H activation cannot be ruled out on the basis of the first key step in the catalytic cycle.

Since clarity on whether *ortho* C–H activation is more likely than that at the *para* position under the experimental conditions could not be sought on the basis of the computed energetics of the C–H activation step, we have carefully examined the ensuing steps of the catalytic cycle in greater detail. Interestingly, the Ir(v)-aryl intermediate (**2**) formed as a result of the C–H activation at the *ortho* as well as *para* positions is found to be more reversible than the one derived at the *meta* position.[50] Furthermore, a comparative study of the reductive elimination (RE) leading to the formation of the borylated product is undertaken for the ubpy-**S0** catalyst–substrate combination. An elementary step barrier of 21.5 kcal mol^{-1} is found for the RE to a *meta* borylated product, which is in concert with the experimental preference toward the *meta* product. However, the RE elimination barrier at the *para* position is 27.4 kcal mol^{-1} while that at the *ortho* position is found to be 32.8 kcal mol^{-1}, suggesting that the *para* product would be the next most likely product other than the *meta*, in accord with the experimental observations. Though the pathways appear to compete in the initial oxidative addition step, the application of the energetic span model also helped us understand the regioselectivity more

convincingly.[51] While the TDI is the respective catalyst–substrate complex (**1**) in all these pathways, the TDTS for the *meta* pathway is found to be the oxidative addition and that for the *para* and *ortho* pathways it is the reductive elimination. The corresponding energetic span δE for *para* and *ortho* is, respectively, 27.3 and 32.8 kcal mol^{-1}. In other words, the catalytic turnover toward *ortho* is the least favored, followed by the *para* product. It is also interesting to note that the relative enthalpies of the relevant TSs also convey a similar trend in the predicted selectivities.[52] Thus, the overall energetic features of various borylation pathways suggest the formation of the *meta* product as the major and *para* as the minor regioisomer in this catalytic transformation.[53]

Conclusion

Density functional theory investigation of important Ir(III)-catalyzed *meta* selective aryl C(sp^2)–H borylation revealed that the key mechanistic steps in the lower energy pathway are (i) oxidative addition (C–H activation), (ii) reductive elimination (borylation), and (iii) catalyst regeneration. A comparison of energies and stereoelectronic factors operating in the C–H activation transition states for *meta* and *para* functionalization of *N,N*-dihexylbenzamide helped us gain significant new insights into the role of various noncovalent interactions, particularly between the catalyst and the substrate. The catalyst Ir(III)(ubpy)tris(boryl), decorated with a phenylene-urea tether on the bpy ligand is found to play an important role in positioning the aryl amide through N–H···O H-bonding interactions such that the C–H activation at the *meta* position is rendered energetically more favorable over that at *para*. However, we noted that the presence or absence of this H-bonding interaction could not solely account for the regioselectivity. A good number of noncovalent interactions between the catalyst (Ir-bound ligands) and the substrate are found to be vital toward bringing about the energy difference between the *meta* and *para* C–H activation TSs. These interactions, operating between the C–H bonds of the substrate (hexyl and aryl moieties) and (i) the bipyridyl nitrogen atoms as well as the π-face of the Ir-bound ubpy ligand and (ii) the oxygen atoms of B$_2$pin$_2$, are found to be more prominent in the *meta* C–H activation transition state, thereby making it 6.6 kcal mol^{-1} lower in energy than the *para* analogue. This energy difference is fully consistent with the experimental observation of the high *meta* to *para* ratio of 27.

Additional series of computations on modified systems obtained by changing the substrate (replacing dihexyl with dimethyl), catalysts without the urea moiety on the Ir-bound ubpy ligand, and the use of B$_2$(OMe)$_4$ instead of B$_2$pin$_2$ as the borylating agent further helped us conclude that the balance between C–H···π, C–H···O and C–H···N NCIs that operate between the catalyst and the substrate is more important than the primary N–H···O H-bonding contact that binds the substrate to the catalyst. For instance, the *meta* C–H activation TS for the *N,N*-dimethylbenzamide is noted to enjoy a larger number of relatively better NCIs thereby maintaining high regioselectivity even though the C–H···π interactions are not as much as those in *N,N*-dihexylbenzamide. For the catalysts

devoid of N–H···O interactions (bpy and dtbpy), the low selectivity could be attributed to the absence of differentiating NCIs between the *meta* and the *para* TSs. With the modified borylating agent, the predicted lower selectivity relative to the parent system is found to be due to the presence of similar efficiencies in the C–H···O and C–H···N interactions in the *para* TS to those in the *meta* TS. The regioselectivity of the borylation reaction thus hinges upon a set of NCIs that operate in concert and hence could be fine-tuned by making a rational choice of the ligand on the catalyst and suitable reactants. These conclusions are expected to have broader applicability in developing catalytic regioselective protocols using noncovalent interactions.

Conflicts of interest

There are no conflicts to declare.

Acknowledgements

Notes and references

1 (a) N. Miyaura and A. Suzuki, *Chem. Rev.*, 1995, **95**, 2457–2483; (b) J. Simon, S. Salzbrunn, G. K. S. Prakash, N. A. Petasis and G. A. Olah, *J. Org. Chem.*, 2001, **66**, 633–634; (c) J. F. Hartwig, *Acc. Chem. Res.*, 2012, **45**, 864–873.

2 (a) J. He, M. Wasa, K. S. L. Chan, Q. Shao and J.-Q. Yu, *Chem. Rev.*, 2017, **117**, 8754–8786; (b) R.-Y. Zhu, M. E. Farmer, Y.-Q. Chen and J.-Q. Yu, *Angew. Chem., Int. Ed. Engl.*, 2016, **55**, 10578–10599; (c) Z. Dong, Z. Ren, S. J. Thompson, Y. Xu and G. Dong, *Chem. Rev.*, 2017, **117**, 9333–9403; (d) Y. Park, Y. Kim and S. Chang, *Chem. Rev.*, 2017, **117**, 9247–9301; (e) J. R. Hummel, J. A. Boerth and J. A. Ellman, *Chem. Rev.*, 2017, **117**, 9163–9227; (f) C. Patel, V. Abraham and R. B. Sunoj, *Organometallics*, 2017, **36**, 151–158.

3 (a) T. Ishiyama, J. Takagi, K. Ishida, N. Miyaura, N. R. Anastasi and J. F. Hartwig, *J. Am. Chem. Soc.*, 2002, **124**, 390–391; (b) H. Tamura, H. Yamazaki, H. Sato and S. Sakaki, *J. Am. Chem. Soc.*, 2003, **125**, 16114–16126; (c) G. A. Chotana, B. A. Vanchura II, M. K. Tse, R. J. Staples, R. E. Maleczka Jr and M. R. Smith III, *Chem. Commun.*, 2009, **0**, 5731–5733.

4 (a) T. A. Boebel and J. F. Hartwig, *J. Am. Chem. Soc.*, 2008, **130**, 7534–7535; (b) T. Ishiyama, H. Isou, T. Kikuchi and N. Miyaura, *Chem. Commun.*, 2010, **46**, 159–161; (c) P. C. Roosen, V. A. Kallepalli, B. Chattopadhyay, D. A. Singleton, R. E. Maleczka and M. R. Smith, *J. Am. Chem. Soc.*, 2012, **134**, 11350–11353; (d) A. Ros, R. Fernández and J. M. Lassaletta, *Chem. Soc. Rev.*, 2014, **43**, 3229–3243.

5 (a) J.-Y. Cho, M. K. Tse, D. Holmes, R. E. Maleczka and M. R. Smith, *Science*, 2002, **295**, 305–308; (b) T. Ishiyama, J. Takagi, J. F. Hartwig and N. Miyaura, *Angew. Chem., Int. Ed. Engl.*, 2002, **41**, 3056–3058; (c) R. J. Phipps and M. J. Gaunt, *Science*, 2009, **323**, 1593–1597; (d) B. Chen, X.-L. Hou, Y.-X. Li and Y.-D. Wu, *J. Am. Chem. Soc.*, 2011, **133**, 7668–7671; (e) N. Hofmann and L. Ackermann, *J. Am. Chem. Soc.*, 2013, **135**, 5877–5884; (f) C. Cheng and J. F. Hartwig, *Science*, 2014, **343**, 853–857; (g) Y.-F. Yang, G.-J. Cheng, P. Liu, D. Leow, T.-Y. Sun, P. Chen, X. Zhang, J.-Q. Yu, Y.-D. Wu and K. N. Houk, *J. Am. Chem. Soc.*, 2014, **136**, 344–355; (h) Q. Yu, L. Hu, Y. Wang, S. Zheng and J. Huang, *Angew. Chem., Int. Ed. Engl.*, 2015, **54**, 15284–15288; (i) Z. Dong, J. Wang and G. Dong, *J. Am. Chem. Soc.*, 2015, **137**, 5887–5890; (j) S. Li, L. Cai, H. Ji, L. Yang and G. Li, *Nat. Commun.*, 2016, **7**, 10443.

6 J. Li, S. Warratz, D. Zell, S. De Sarkar, E. E. Ishikawa and L. Ackermann, *J. Am. Chem. Soc.*, 2015, **137**, 13894–13901.

7 (a) K. M. Engle and J.-Q. Yu, *J. Org. Chem.*, 2013, **78**, 8927–8955; (b) P. Wang, P. Verma, G. Xia, J. Shi, J. X. Qiao, S. Tao, P. T. W. Cheng, M. A. Poss, M. E. Farmer, K.-S. Yeung and J.-Q. Yu, *Nature*, 2017, **551**, 489–493.

8 Applicable to C(sp^3)–H activation: (a) G. Chen, Z. Zhuang, G.-C. Li, T. G. Saint-Denis, Y. Hsiao, C. L. Joe and J.-Q. Yu, *Angew. Chem., Int. Ed. Engl.*, 2017, **56**, 1506–1509; (b) R.-Y. Zhu, T. G. Saint-Denis, Y. Shao, J. He, J. D. Sieber, C. H. Senanayake and J.-Q. Yu, *J. Am. Chem. Soc.*, 2017, **139**, 5724–5727.

9 (a) K. Müller-Dethlefs and P. Hobza, *Chem. Rev.*, 2000, **100**, 143–168; (b) R. R. Knowles and E. N. Jacobsen, *Proc. Natl. Acad. Sci. U. S. A.*, 2010, **107**, 20678–20685; (c) O. Takahashi, Y. Kohno and M. Nishio, *Chem. Rev.*, 2010, **110**, 6049–6076; (d) M. J. Plevin, D. L. Bryce and J. Boisbouvier, *Nat. Chem.*, 2010, **2**, 466–471; (e) L. M. Salonen, M. Ellermann and F. Diederich, *Angew. Chem., Int. Ed. Engl.*, 2011, **50**, 4808–4842.

10 (a) A. J. Neel, M. J. Hilton, M. S. Sigman and F. D. Toste, *Nature*, 2017, **543**, 637–646; (b) J. P. Wagner and P. R. Schreiner, *Angew. Chem., Int. Ed. Engl.*, 2015, **54**, 12274–12296; (c) S. E. Wheeler, T. J. Seguin, Y. Guan and A. C. Doney, *Acc. Chem. Res.*, 2016, **49**, 1061–1069; (d) R. B. Sunoj, *Acc. Chem. Res.*, 2016, **49**, 1019–1028.

11 (a) Y. Kuninobu, H. Ida, M. Nishi and M. Kanai, *Nat. Chem.*, 2015, **7**, 712–717; (b) H. L. Li, Y. Kuninobu and M. Kanai, *Angew. Chem., Int. Ed. Engl.*, 2017, **56**, 1495–1499.

12 (a) R. Bisht and B. Chattopadhyay, *J. Am. Chem. Soc.*, 2016, **138**, 84–87; (b) M. E. Hoque, R. Bisht, C. Haldar and B. Chattopadhyay, *J. Am. Chem. Soc.*, 2017, **139**, 7745–7748; (c) M. R. Smith, R. Bisht, C. Haldar, G. Pandey, J. E. Dannatt, B. Ghaffari, R. E. Maleczka and B. Chattopadhyay, *ACS Catal.*, 2018, **8**, 6216–6223.

13 (a) H. J. Davis, M. T. Mihai and R. J. Phipps, *J. Am. Chem. Soc.*, 2016, **138**, 12759–12762; (b) H. J. Davis and R. J. Phipps, *Chem. Sci.*, 2017, **8**, 864–877; (c) M. T. Mihai, H. J. Davis, G. R. Genov and R. J. Phipps, *ACS Catal.*, 2018, **8**, 3764–3769.

14 (a) M. Anand, R. B. Sunoj and H. F. Schaefer, *ACS Catal.*, 2016, **6**, 696–708; (b) U. Dutta, A. Modak, B. Bhaskararao,

M. Bera, S. Bag, A. Mondal, D. W. Lupton, R. B. Sunoj and D. Maiti, *ACS Catal.*, 2017, **7**, 3162–3168; (*c*) S. Singh, S. K and R. B. Sunoj, *J. Org. Chem.*, 2017, **82**, 9619–9626; (*d*) A. Deb, S. Singh, K. Seth, S. Pimparkar, B. Bhaskararao, S. Guin, R. B. Sunoj and D. Maiti, *ACS Catal.*, 2017, **7**, 8171–8175; (*e*) C. Athira and R. B. Sunoj, *Org. Biomol. Chem.*, 2016, **15**, 246–255; (*f*) C. Athira, A. Changotra and R. B. Sunoj, *J. Org. Chem.*, 2018, **83**, 2627–2639.

15 Y. Kuninobu, H. Ida, M. Nishi and M. Kanai, *Nat. Chem.*, 2015, **7**, 712–717.

16 M. J. Frisch, G. W. Trucks, H. B. Schlegel, G. E. Scuseria, M. A. Robb, J. R. Cheeseman, G. Scalmani, V. Barone, B. Mennucci, G. A. Petersson, H. Nakatsuji, M. Caricato, X. Li, H. P. Hratchian, A. F. Izmaylov, J. Bloino, G. Zheng, J. L. Sonnenberg, M. Hada, M. Ehara, K. Toyota, R. Fukuda, J. Hasegawa, M. Ishida, T. Nakajima, Y. Honda, O. Kitao, H. Nakai, T. Vreven, J. A. Montgomery Jr, J. E. Peralta, F. Ogliaro, M. Bearpark, J. J. Heyd, E. Brothers, K. N. Kudin, V. N. Staroverov, T. Keith, R. Kobayashi, J. Normand, K. Raghavachari, A. Rendell, J. C. Burant, S. S. Iyengar, J. Tomasi, M. Cossi, N. Rega, J. M. Millam, M. Klene, J. E. Knox, J. B. Cross, V. Bakken, C. Adamo, J. Jaramillo, R. Gomperts, R. E. Stratmann, O. Yazyev, A. J. Austin, R. Cammi, C. Pomelli, J. W. Ochterski, R. L. Martin, K. Morokuma, V. G. Zakrzewski, G. A. Voth, P. Salvador, J. J. Dannenberg, S. Dapprich, A. D. Daniels, O. Farkas, J. B. Foresman, J. V. Ortiz, J. Cioslowski, and D. J. Fox, *Gaussian 09, Revision D.01*, Gaussian, Inc., Wallingford CT, 2013.

17 (*a*) A. D. Becke, *Phys. Rev. A*, 1988, **38**, 3098–3100; (*b*) C. Lee, W. Yang and R. G. Parr, *Phys. Rev. B: Condens. Matter Mater. Phys.*, 1988, **37**, 785–789.

18 S. Grimme, J. Antony, S. Ehrlich and H. Krieg, *J. Chem. Phys.*, 2010, **132**, 154104.

19 (*a*) P. Fuentealba, H. Stoll, L. von Szentpaly, P. Schwerdtfeger and H. Preuss, *J. Phys. B: At. Mol. Phys.*, 1983, **16**, L323–L328; (*b*) D. Andrae, U. Häußermann, M. Dolg, H. Stoll and H. Preuß, *Theor. Chim. Acta*, 1990, **77**, 123–141.

20 (*a*) P. C. Hariharan and J. A. Pople, *Theor. Chim. Acta*, 1973, **28**, 213–222; (*b*) M. M. Francl, W. J. Pietro, W. J. Hehre, J. S. Binkley, M. S. Gordon, D. J. DeFrees and J. A. Pople, *J. Chem. Phys.*, 1982, **77**, 3654–3665; (*c*) V. A. Rassolov, J. A. Pople, M. A. Ratner and T. L. Windus, *J. Chem. Phys.*, 1998, **109**, 1223–1229; (*d*) V. A. Rassolov, M. A. Ratner, J. A. Pople, P. C. Redfern and L. A. Curtiss, *J. Comput. Chem.*, 2001, **22**, 976–984.

21 (*a*) B. Chattopadhyay, J. E. Dannatt, I. L. Andujar-De Sanctis, K. A. Gore, R. E. Maleczka, D. A. Singleton and M. R. Smith, *J. Am. Chem. Soc.*, 2017, **139**, 7864–7871; (*b*) A. Guðmundsson, K. P. J. Gustafson, B. K. Mai, B. Yang, F. Himo and J.-E. Bäckvall, *ACS Catal.*, 2018, **8**, 12–16; (*c*) B. Tutkowski, S. Kerdphon, E. Limé, P. Helquist, P. G. Andersson, O. Wiest and P.-O. Norrby, *ACS Catal.*, 2018, **8**, 615–623; (*d*) S. Chen, X. Huang, E. Meggers and K. N. Houk, *J. Am. Chem. Soc.*, 2017, **139**, 17902–17907.

22 (*a*) K. Fukui, *Acc. Chem. Res.*, 1981, **14**, 363–368; (*b*) C. Gonzalez and H. B. Schlegel, *J. Chem. Phys.*, 1998, **90**, 2154.

23 A. V. Marenich, C. J. Cramer and D. G. Truhlar, *J. Phys. Chem. B*, 2009, **113**, 6378–6396.

24 S. Grimme, *Chem.–Eur. J.*, 2012, **18**, 9955–9964.

25 (*a*) R. F. W. Bader, *Atoms in Molecules: A Quantum Theory*, Oxford University Press, Oxford, New York, 1994; (*b*) *AIM2000 Version 2.0*, Buro fur Innovative Software, SBK Software: Bielefeld, Germany, 2002; (*c*) F. Biegler-König and J. Schönbohm, *J. Comput. Chem.*, 2001, **22**, 545–559; (*d*) F. Biegler-König and J. Schönbohm, *J. Comput. Chem.*, 2002, **23**, 1489–1494.

26 E. R. Johnson, S. Keinan, P. Mori-Sánchez, J. Contreras-García, A. J. Cohen and W. Yang, *J. Am. Chem. Soc.*, 2010, **132**, 6498–6506.

27 S. Kozuch and S. Shaik, *Acc. Chem. Res.*, 2011, **44**, 101–110.

28 For more details of Ir(III)(bpy)tris(boryl) as an active catalyst, see: (*a*) T. M. Boller, J. M. Murphy, M. Hapke, T. Ishiyama, N. Miyaura and J. F. Hartwig, *J. Am. Chem. Soc.*, 2005, **127**, 14263–14278; B. A. Vanchura II, S. M. Preshlock, P. C. Roosen, V. A. Kallepalli, R. J. Staples, R. E. Maleczka Jr, D. A. Singleton and M. R. Smith III, *Chem. Commun.*, 2010, **46**, 7724–7726. (*c*) P. C. Roosen, V. A. Kallepalli, B. Chattopadhyay, D. A. Singleton, R. E. Maleczka and M. R. Smith, *J. Am. Chem. Soc.*, 2012, **134**, 11350–11353; (*d*) Q. Li, C. W. Liskey and J. F. Hartwig, *J. Am. Chem. Soc.*, 2014, **136**, 8755–8765.

29 (*a*) In the model system, the cyclohexane (Cy) of the ligand and the *N*-hexyl chain of the substrate are replaced by a methyl group and the borylating reagent B_2pin_2 is replaced by bis(ethyleneglycolato)diboron (B_2eg_2); (*b*) More details are provided in Fig. S1 in the ESI.†; (*c*) In the most favored geometry of the active catalyst, N–H···O interactions between the oxygen atom of the Beg (from B_2eg_2) ligand and the N–Hs of the urea bring the urea moiety closer to the Beg; (*d*) Two key configurations of the active catalyst, with and without the N–H···O interactions differ by about 6 kcal mol^{-1}. See Fig. S2 in the ESI† for further details.

30 In addition, the *meta* C–H activation TS obtained from the energetically favored geometry of the active catalyst (**A1**) differed by around 12 kcal mol^{-1} relative to the one obtained from **A2**. See Fig. S8 in the ESI.†

31 See Fig. S3 in the ESI.†

32 The most favorable arrangement of the catalyst-substrate complex along with their computed energies is shown in Fig. S4 in the ESI.†

33 (*a*) The optimized geometries of the catalyst-substrate complex in different binding modes are provided in Fig. S5 in the ESI.†; (*b*) Interesting strategies, such as template assisted distal functionalization, have been developed to access distal *meta* and *para* positions of aryl rings, see: ; (*c*) D. Leow, G. Li, T.-S. Mei and J.-Q. Yu, *Nature*, 2012, **486**, 518–522; (*d*) A. Maji, B. Bhaskararao, S. Singha, R. B. Sunoj and D. Maiti, *Chem. Sci.*, 2016, **7**, 3147–3153; (*e*) Y. Wu, Y.-Q. Chen, T. Liu, M. D. Eastgate and J.-Q. Yu, *J. Am.*

Chem. Soc., 2016, **138**, 14554–14557; (*f*) X.-H. Liu, H. Park, J.-H. Hu, Y. Hu, Q.-L. Zhang, B.-L. Wang, B. Sun, K.-S. Yeung, F.-L. Zhang and J.-Q. Yu, *J. Am. Chem. Soc.*, 2017, **139**, 888–896; (*g*) H.-J. Xu, Y. Lu, M. E. Farmer, H.-W. Wang, D. Zhao, Y.-S. Kang, W.-Y. Sun and J.-Q. Yu, *J. Am. Chem. Soc.*, 2017, **139**, 2200–2203; (*h*) Z. Zhang, K. Tanaka and J.-Q. Yu, *Nature*, 2017, **543**, 538–542; (*i*) A. Maji, S. Guin, S. Feng, A. Dahiya, V. K. Singh, P. Liu and D. Maiti, *Angew. Chem., Int. Ed. Engl.*, 2017, **56**, 14903–14907

34 (*a*) The energies of the C–H activation TSs in the solvent phase for the model system with Ir···π and Ir···N modes of binding are, respectively, 1.1 and 0.7 kcal mol^{-1} less favored over the Ir···O binding. A similar trend is also found for the corresponding activation barriers (∼26 to 27 kcal mol^{-1}), suggesting that all the three binding modes could facilitate C–H activation at the *ortho* position; (*b*) The optimized TS geometries for the *ortho* C–H activation in all three modes of the model system are given in Fig. S6 in the ESI.†

35 The details of conformational sampling of the transition state geometries, particularly arising due to the long hexyl chains, are presented in Tables S1–S5 in the ESI.†

36 The optimized TS geometries for all the steps are provided in the ESI (Fig. S7†).

37 (*a*) To obtain the maximum δE, different likely stationary points involved in the catalytic cycle are considered as the TDTS and TDI. More details are provided in Table S6 in the ESI.†; (*b*) The turn-over frequency estimated using the calculated δE is found to be 4.8 × 10^{-4} s^{-1}; (*c*) S. Kozuch and J. M. L. Martin, *ACS Catal.*, 2012, **2**, 2787–2794

38 E. Espinosa, I. Alkorta, J. Elguero and E. Molins, *J. Chem. Phys.*, 2002, **117**, 5529.

39 The details of the important NCIs as identified through the AIM analysis along with their energetic contribution calculated using Espinosa's formulation for the systems, ubpy-**S0** and ubpy-**S1**, are presented in Table S7 in the ESI.†

40 Additional depiction of all these noncovalent interactions is provided in the form of NCI plots in Fig. S9 in the ESI.†

41 F. M. Bickelhaupt and K. N. Houk, *Angew. Chem., Int. Ed. Engl.*, 2017, **56**, 10070–10086.

42 The details of the DI-AS analysis are provided in Fig. S10 and Table S8 in the ESI.†

43 (*a*) P. T. Brain, A. J. Downs, P. Maccallum, D. W. H. Rankin, H. E. Robertson and G. A. Forsyth, *J. Chem. Soc., Dalton Trans.*, 1991, **0**, 1195–1200; (*b*) H. Braunschweig and A. Damme, *Chem. Commun.*, 2013, **49**, 5216–5218; (*c*) H. Kinuta, H. Takahashi, M. Tobisu, S. Mori and N. Chatani, *Bull. Chem. Soc. Jpn.*, 2014, **87**, 655–669; (*d*) F. Haeffner, *Comput. Theor. Chem.*, 2018, **1131**, 90–98.

44 (*a*) The predicted low regioselectivity is comparable to the closest experimental observation wherein Ir-dtbpy, devoid of the phenyl-urea linker yielded a *meta* to *para* ratio of 1.9. Our calculations of the dtbpy-**S0** system also indicated an energy difference of only 0.4 kcal mol^{-1} in favor of *meta*

C–H activation; (*b*) The *meta* and *para* C–H activation TS geometries for the dtbpy-**S0** system are given in Fig. S11 in the ESI.†

45 The *meta* and *para* C–H activation TS geometries with a modified Ir-bound ligand (bpy) as well as with a modified borylating agent (**B1**) are given in Fig. S12 in the ESI.†

46 Relative enthalpy and free energy differences between the *meta* and *para* C–H activation TSs for the modified and unmodified systems are presented in Table S9 in the ESI.†

47 (*a*) The relative strengths of all the important NCIs in terms of their individual energetic contribution for the ligand bpy and the borylating agent **B1** are provided in Table S10 in the ESI.†; (*b*) The bar diagrams for bpy and **B1** systems are given in Fig. S13 in the ESI.†

48 The details of the DI-AS analysis for dtbpy, bpy and **B1** modifications are provided in Tables S11–S13 in the ESI.†

49 (*a*) The calculations were also performed with a much larger basis set, 6-311++G**, for all atoms except for iridium, for which LANL2TZ(f) was used; (*b*) The details are provided in Table S14 in the ESI.† Various levels of theories were consistent in conveying the *meta* C–H activation as the most favored site of activation followed by *ortho* and *para* positions.

50 (*a*) See Fig. S14 and S15 in the ESI† for Gibbs free energy profiles of *para* and *ortho* borylations; (*b*) The C–H activation step in the *ortho* and *para* pathways is found to be more reversible toward the reactants. The barriers for the reversal of the Ir(v)-aryl intermediate (**2**) are 6.7 and 4.6 kcal mol^{-1}, respectively, for *ortho* and *para* intermediates. The corresponding value of the *meta* intermediate is 8.5 kcal mol^{-1}. The elementary step barriers for the forward reaction (*i.e.*, the reductive elimination from **2$_o$** and **2$_p$**) in the *ortho* and *para* pathways are, respectively, 15.7 and 6.6 kcal mol^{-1}, suggesting that *ortho* borylation is least likely. Thus, *para* borylation is the only alternative possibility other than the *meta* product.

51 (*a*) To obtain a maximum δE, different likely stationary points involved in the catalytic cycle for both the *para* and *ortho* pathways are considered as the TDTS and TDI. See Table S15 and S16 in the ESI† for additional details; (*b*) The turn-over frequency estimated using the calculated δE is found to be 5.6 × 10^{-8} and 5.3 × 10^{-12} s^{-1}, respectively, for the *para* and *ortho* isomers.

52 The enthalpies of formation of *meta*, *ortho* and *para* borylated products are summarized in Table S17 in the ESI.†

53 (*a*) Energy profile diagram of the oxidative addition and RE steps for three isomers are given in Fig. S16 in the ESI.†; (*b*) The energy of the catalyst-substrate complex in each case differs by about 4 kcal mol^{-1}. See Fig. S15 in the ESI† for additional details; (*c*) Calculations at other higher levels of theories for RE in the case of *meta*, *ortho* and *para* isomers are presented in Table S18 in ESI.†